Interpenetrated hydrogels composed of cellulose nanocrystals and biosurfactants

Thuy-Linh Phi, Niki Baccile, Eero Kontturi

Interpenetrated hydrogels composed of cellulose nanocrystals and biosurfactants

Thuy-Linh Phi [a,b] , Niki Baccile [a,], Eero Kontturi [b,*]*

[a] Sorbonne Université, Centre National de la Recherche Scientifique, Laboratoire de Chimie de la Matière Condensée de Paris, LCMCP, F-75005 Paris, France

[b] Department of Bioproducts and Biosystems, School of Chemical Engineering, Aalto University, P.O. Box 16300, 00076 Aalto, Finland

Highlights

KEYWORDS: cellulose nanocrystal, biosurfactant, hydrogel

ABSTRACT (Word Style "BD_Abstract"). All manuscripts must be accompanied by an abstract. The abstract should briefly state the problem or purpose of the research, indicate the theoretical or experimental plan used, summarize the principal findings, and point out major conclusions. Abstract length is one paragraph.

TABLE OF CONTENT FIGURE

Introduction

Start by hydrogel -> bioS -> CNC

Hydrogels are three-dimensional networks composed of either natural or synthetic hydrophobic polymers, possess the remarkable ability to retain significant volumes of aqueous solutions while maintaining their original structure. In general, hydrogels, which are highly hydrated cross-linked three-dimensional networks, can be prepared by either using chemical or physical cross-linking techniques and encompass a wide range of chemical compositions and structural forms.[1,2] This characteristic renders them versatile for applications across various fields, including biomedicine [3–5] and food industry, [6,7] where their biocompatibility, biodegradable, and unique rheological features are exploited. In this research, a composite system, where low-molecular weight gelators (LMWGs) serve as the hydrogel matrix, while cellulose nanocrystals (CNCs) function as insoluble fillers is investigated.

Low-molecular-weight gelators (LMWGs) are small molecules with a molecular weight less than approximately 1 kDa, capable of forming self-assembled fibrillar network (SAFiN) hydrogels in water. [8] The majority of SAFiN gels are characterized by an entangled network of self-assembled fibers, akin to a polymer in a favorable solvent. These LMWGs are engineered to exhibit intriguing self-assembly behavior driven by non-covalent interactions, allowing for a supramolecular assembly process that can be adjusted [9,10] to form a gel more or less reversibly. [8,11,12] This study focused on the SAFiN hydrogels made entirely from a bolaform glycolipid with an oleic acid (C18:1) backbone. The compound, G-C18:1, derived from fermentation of natural resources, exhibits a triple surfactant-lipid-gelator nature **(**Erreur ! Source du renvoi introuvable.**)**.[13] Below neutral pH and at concentrations under 5 wt%, G-C18:1 form vesicle, displaying lipid-like behavior. [14,15] At pH levels above neutral, it transitions to micelle formation, demonstrating surfactant behavior.[14,15] In the presence of micelles and metal ions, it can form either wormlike micelles or fibers, depending on the chemical nature of the ion.[16] The micelle-to-fiber transition is triggered at pH levels above neutral through the addition of specific cations (Ca^{2+}, Ag^{+}, Mn^{2+}) **(**Erreur ! Source du renvoi introuvable.**)**.[16] This cation-induced

fibrillation is novel not only for this compound but also for other biosurfactants,[17–19] and is generally unexpected in surfactant solutions, which typically exhibit micelle-to-cylinder,[20–23] -wormlike,[24] -vesicle[25] or -lamellar[20] transitions when mixed with mono- or multivalent cations.

In this study, SAFiN hydrogels have been investigated in the presence of cellulose nanocrystals (CNCs). These rod-like nanocrystalline cellulose particles have garnered extensive attention due to its unique features, such as high strength, high elastic modulus, hydrophilicity, and light weight. [26–32] The potential leading material of the green economy can be extracted from various renewable biomass (e.g., cotton, wood, bacteria, and sea tunicates, etc.) sources through acid hydrolysis process of cellulose fibers, resulted in varied surface charge and size of the nanocrystals ranging from hundreds of nanometers to several microns. [33–41] Importantly, CNCs are environmentally friendly (i.e., non-toxicity, renewability, and biodegradability), abundant in nature, and inexpensive. [42] CNCs are typically extracted by acid hydrolysis using sulfuric acid which causes the crystal surface to be negatively charged due to the fact that a fraction of the surface hydroxyl groups is esterified to sulfate half-ester groups. [36,43,44] However, it is important to note that there are other acids employed for acid hydrolysis, including hydrochloric acid, nitric acid and phosphoric acid. [45–47] Additionally, alternative methods for obtaining CNCs exist, such as mechanical treatments, [35,48] ionic liquid hydrolysis, [49] vapor and gaseous acid hydrolysis. [50–52] It is noteworthy that the native cellulose surface is unstable and promote the self-aggregation due to the hydrogen bonding between these -OH groups.[29,53] Current strategies to improve cellulose particle dispersibility and isolation focus on increasing charge repulsion and steric hindrance through surface modification. [54,55] Nanocellulose surfaces have been modified through simple reactions, like oxidation, [56–58] esterification, [59–61] and acetylation, [62,63] among others. These modifications, which sometimes include grafting polymers [64,65] or other functional materials [66–68] or low-molecular weight such as surfactants [69–72] have attracted great attention across several applications, including biomedical devices, food modifiers and cosmetic materials. [73]
Over the past 15 years, cellulose nanocrystals (CNCs) have gained attention as reinforcement agents in hydrogels and nanocomposites, improving mechanical properties and stability. [74–77] CNCs have been incorporated into synthetic and natural polymer matrices, such as PVA, [78–80] PAM,[81–83] PEG,[84,85] alginate,[86] and gelatin,[77] among others.[76,87–92] Their good dispersibility and ability to enhance stress transfer make them effective in strengthening hydrogels,[93,94] with applications in biomedical fields. [95,96]

The aim of this research is to enhance our comprehension of how the incorporation of cellulose nanocrystals (CNCs) influences the structural and rheological characteristics of SAFiN hydrogels, particularly emphasizing the reinforcing impact introduced by cellulosic nanofillers (Erreur ! Source du renvoi introuvable.). From a practical perspective, this study endeavors to design novel eco-friendly hydrogels with superior mechanical properties.

Materials and Methods

Chemicals.

Monounsaturated glucolipid G-C18:1 (molecular weight 461 g/mol) was obtained from Amphistar in Gent, Belgium, and produced at the Bio Base Europe Pilot Plant in Gent, Belgium, under batch No. APS F06/F07, Inv96/98/99. According to the supplier, the batch, with 99.4% dry matter, was predominantly composed of 99.5% G-C18:1. The molecule was synthesized through fermentation using the yeast strain Starmerella bombicola ΔugtB1, as per a previously established protocol. [97] It was used in its

original form. To adjust the pH, sodium hydroxide and hydrochloric acid solutions (Sigma-Aldrich, Germany) were used. The gelation of G-C18:1 was trigged by $CaCl_2$ (VWR). Whatman 1 filter papers (Catalog No. 1001 150), were used as cellulose substrate. According to the manufacturer, these filter papers are primarily made from purified cotton linters, with a cellulose content exceeding 98%. Hydrochloric acid liquid (~37% concentration, Sigma-Aldrich) was used from a concentrated stock solution. HCl gas (99.8%, 10 dm^3, 6 kg) was purchased from AGA (Sweden). High sulfur content cellulose nanocrystals (H_2SO_4-CNC), with widths of 10–20 nm and lengths of 300–900 nm, obtained from Nanografi in Turkey, were used as reference materials. For all dilution, washing, and rinsing steps, Milli-Q water was used.

Hydrolysis with liquid HCl. The preparation of cellulose nanocrystals with liquid HCl (LCNC) in a conventional liquid-solid system followed the method described by Klemm *et al.,*.[98] To start, 10 grams of Whatman 1 filter paper were mixed with 300 milliliters of pre-heated 3 M hydrochloric acid (HCl) solution, with continuous stirring at 1500 rpm at 80°C for 4 hours. The resulting suspension was then subjected to multiple rounds of centrifugation at 1460 g (2900 rpm) for 10 minutes each, until the pH reached between 4 and 5. Afterward, the solution was dialyzed for three days using a Spectra/Por® Dialysis Membrane (molecular weight cutoff 6-8 kD, part number 132665).

Hydrolysis with gaseous HCl. CNCs hydrolysis with HCl gas (GCNC) was carried out in a custom-built reactor, following the method of Kontturi *et al.,*.[52] Ten grams of Whatman 1 filter paper were placed in the reactor, which was degassed to reach the HCl gas pressure of 1 bar. After 19 hours, the gas pressure in the reactor was released, and the sample was immediately weighed and washed with Millipore water (2 × 15 min, 300 ml). The sample was then dehydrated to a dry matter content of over 90% by leaving it overnight in a fume hood at room temperature.

Stabilized CNC after HCl hydrolysis. Both LCNCs and GCNCs require an additional isolation step, as these CNCs lack sufficient repulsive interactions, leading to aggregation.[29,53] First, a 10 mL solution of CNCs at the desired concentration was prepared and subjected to tip sonication (UP200Ht, Hielscher) at 100 W power and 20% amplitude for 10 minutes. Then, a specific amount of G-C18:1 powder was weighed (with CNC:G-C18:1 ratios of 1:1 or 1:0.2) and added to the pre-prepared CNC solutions. The mixture was tip-sonicated again at 10% amplitude for 5 minutes until a homogeneous solution was achieved.

Gels preparation. A stock solution of G-C18:1 at 4 wt% and pH 8.3-8.5 was prepared. Various concentrations of CNCs were added to the G-C18:1 solution, and gelation was initiated by the final addition of $CaCl_2$, with a Ca^{2+} to G-C18:1 ratio of 0.5.

Rheology. An MCR 302 rheometer (Anton Paar, Graz, Austria) with sand-blasted plate-plate geometry (Ø: 25 mm) was used, maintained at a constant temperature of 25°C. A solvent trap containing water was employed to reduce evaporation. Approximately 0.5 mL of gel was carefully placed in the center of the plate with a spatula to avoid trapping air bubbles, and any excess gel was meticulously removed.

SAXS. SAXS measurements were performed at the Sorbone using a Xenocs Xeuss 1.0 laboratory beamline. The instrument employed a Cu source with a wavelength of 1.54 Å and a detector distance

of 310 mm and 2500 mm. High-resolution measurements were obtained with S1 = 0.8 and S2 = 0.5, and an exposure time of 1200 seconds was used.

Rheo-SAXS. Small-Angle X-ray Scattering (SAXS) experiments combined with rheology (Rheo-SAXS) were conducted at the SWING beamline at Synchrotron Soleil, Saint-Aubain, France (Proposal No. 20231446). The beamline operates at an energy of E = 12 keV, with sample-to-detector distances fixed at 2 m and 6 m. The raw data from the 2D detector are azimuthally integrated using the Foxtrot software available at the beamline to generate the typical scattered intensity I(q) profile. Here, q is the wave vector, defined as $q = 4\pi/\lambda \sin(\theta)$, where 2θ is the scattering angle and λ is the wavelength. Each frame corresponds to a 500 ms exposure time followed by a 9500 ms resting period, resulting in one frame being captured every 10 seconds. A MCR 501 rheometer (Anton Paar, Graz, Austria) equipped with a Couette polycarbonate cell (10 mm diameter, 0.5 mm gap, V = 1.35 mL) was coupled to the beamline and controlled remotely from an external computer in the experimental hutch using Rheoplus/32V3.62 software. The experiments were conducted at 25 °C in a radial configuration, with the X-ray beam aligned along the center of the Couette cell. Rheology and SAXS data collection were manually synchronized, with a time synchronization error of less than 3 seconds.

Results and discussions

The gelation of G-C18:1 is triggered by Ca2+ ion. At 2 wt% and pH 8, G-C18:1 exist in the micelle form. With the presence of Ca2+, G-C18:1 self-assemby into fiber form, therefore having gelation.(ref) The optimal amount of $CaCl_2$ for the G-C18:1 gelation process is discussed elsewhere (ref), with a ratio of $\frac{n_{Ca^{2+}}}{n_{G-C18:1}} = 0.5$ deemed sufficient. Thus, 24 µL of $CaCl_2$ 1M is required to gel a 2 wt% G-C18:1 solution. A study investigating the gelation behavior of 2 wt% G-C18:1 solutions with varying amounts of $CaCl_2$ (10-30 mM) was conducted and the results are shown in **Figure S1a**. Measurements taken 7 days after preparation demonstrated that gelation did not occur at $CaCl_2$ concentrations below 20 µL. Based on these findings, a fixed $CaCl_2$ concentration of 27 µL was chosen for subsequent studies, ensuring gel formation.

In some cases, gels become stiffer over time (ref). The mechanical properties of G-C18:1 gels were tracked over a 2-month period **(Figure S1b)**. During the first 3 days, the storage modulus (G') remained steady at around 35 Pa. However, when measured again 7 days after preparation, the G' value increased to 115 Pa and remained stable for over a month, eventually rising to 275 Pa after 2 months. Therefore, in this study, the combination gels of G-C18:1 and different type of CNCs (from now on will be assigned as G-C18:1/[name]CNC) will be measured at 2 and 7 days. To ensure consistent gel quality, the G-C18:1 solution should be sonicated prior to each use. This is essential to prevent aggregation, which can lead to heterogeneity and affect the rheological properties of the gels (**Figure S2**).

1. *G-C18:1/LCNC and G-C18:1/GCNC*

Initially, the effect of the amount of G-C18:1 used to stabilize uncharged CNCs on the mechanical properties of the gels was investigated. According to our previous work, G-C18:1 exhibits two transition phases: from molecule-to-micelle at 0.025 mg/mL (CAC1) and from micelle-to-vesicle at 0.47 mg/mL (CAC2).(ref) It was also found that G-C18:1 concentrations below 0.4 mg/mL are insufficient to stabilize 1 wt% CNC hydrolyzed by HCl, while 1 mg/mL is excessive.(ref) Therefore, in

this study, a 1 wt% CNC solutions was prepared and then stabilized with either 0.2 mg/mL (S0.2) or 1 mg/mL (S1) of G-C18:1 (**Figure S3**) to observe the effect of stabilized CNC on the viscoelastic properties of G-C18:1 gels.

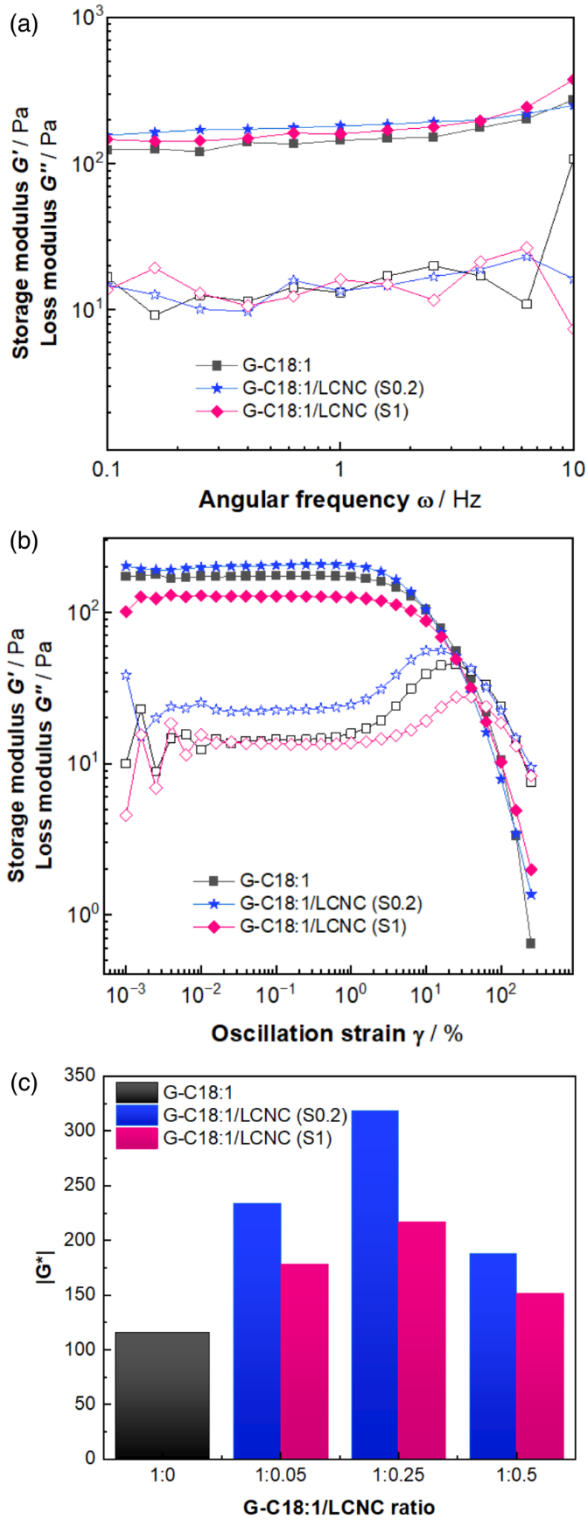

Figure 1. (a) Frequency sweep and (b) Oscillatory strain measurements at 1Hz show the storage G' (full symbols) and loss G'' (empty symbols) moduli for 2 wt% G-C18:1 gels without and with the presence of the same concentration of LCNC, except the different on stabilization of LCNC by G-C18:1; and (c) The

complex shear modulus G of G-C18:1/LCNC gels as a function of the ratio between G-C18:1 matrix (fixed at 2wt%) and LCNC reinforcement.*

Figure 1a and 1b depict the storage modulus (G') and loss modulus (G'') of a G-C18:1 gel and two G-C18:1/LCNC combination gels, prepared using the same method but differing in the amount of G-C18:1 used to stabilize LCNC (S0.2 and S1). These measurements were conducted at day 7. Across the entire frequency range tested (0.1 to 10 Hz), G' consistently exceeded G'', indicating gel-like behavior for all samples. Notably, G-C18:1/LCNC (S0.2) exhibited a consistently higher G' than G-C18:1/LCNC (S1) across all frequencies and strain amplitudes. At 1 Hz, the G' values of the G-C18:1/LCNC gels were 177 Pa (S1) and 232 Pa (S0.2), significantly higher than the G-C18:1 gel (115 Pa) despite the introduction of a small amount of LCNC (ratio 1:0.05). Notably, varying G-C18:1 concentrations below and above the critical aggregation concentration (CAC) did not significantly alter the G' and G'' values. Interestingly, the G" curves show one peak, and the increasing G" values in the partial range indicate the increasing portion of deformation energy, which is spent to change the internal structure before the final break down of the gel structure.(Rheo handbook ref)

To further explore the impact of LCNC concentration as reinforcement in the G-C18:1 gel, the complex modulus (G*) was measured after 7 days and is presented in **Figure 1c**, the oscillatory strain measurements represented in **Figure 2a** and all the data of G' and G'' were reported in **Table S1**. The complex shear modulus (G* = G' + iG"), which reflects the rigidity of a gel under deformation below its yield stress, was consistently higher for G-C18:1/LCNC (S0.2) gels compared to G-C18:1/LCNC (S1) gels. At a G-C18:1 : LCNC ratio of 1:0.25, the maximum G* value for G-C18:1/LCNC (S0.2) was three times greater than that of the G-C18:1 gel demonstrating the beneficial effect of LCNC reinforcement. However, exceeding this optimal ratio resulted in a decrease in gel rigidity, indicating that excessive reinforcement can disrupt the network structure. This reduction in rigidity could be attributed to increased steric hindrance, interference with G-C18:1 self-assembly, or the formation of dense aggregates.

Similar rheological investigations were conducted for G-C18:1/GCNC gels (**Figure 2b)**, with the results for G' and G'' summarized in **Table S2**. No significant differences were observed between G-C18:1/LCNC and G-C18:1/GCNC gels, suggesting that the CNC hydrolysis protocol does not significantly impact the final gel properties. While the optimal matrix-to-reinforcement ratio was found to be 1:0.25, hydrogel formation was achievable at ratios up to 1:1. However, gelation was not possible at a ratio of 1:2, indicating a limit to the amount of CNC that can be effectively incorporated into the hydrogel matrix.

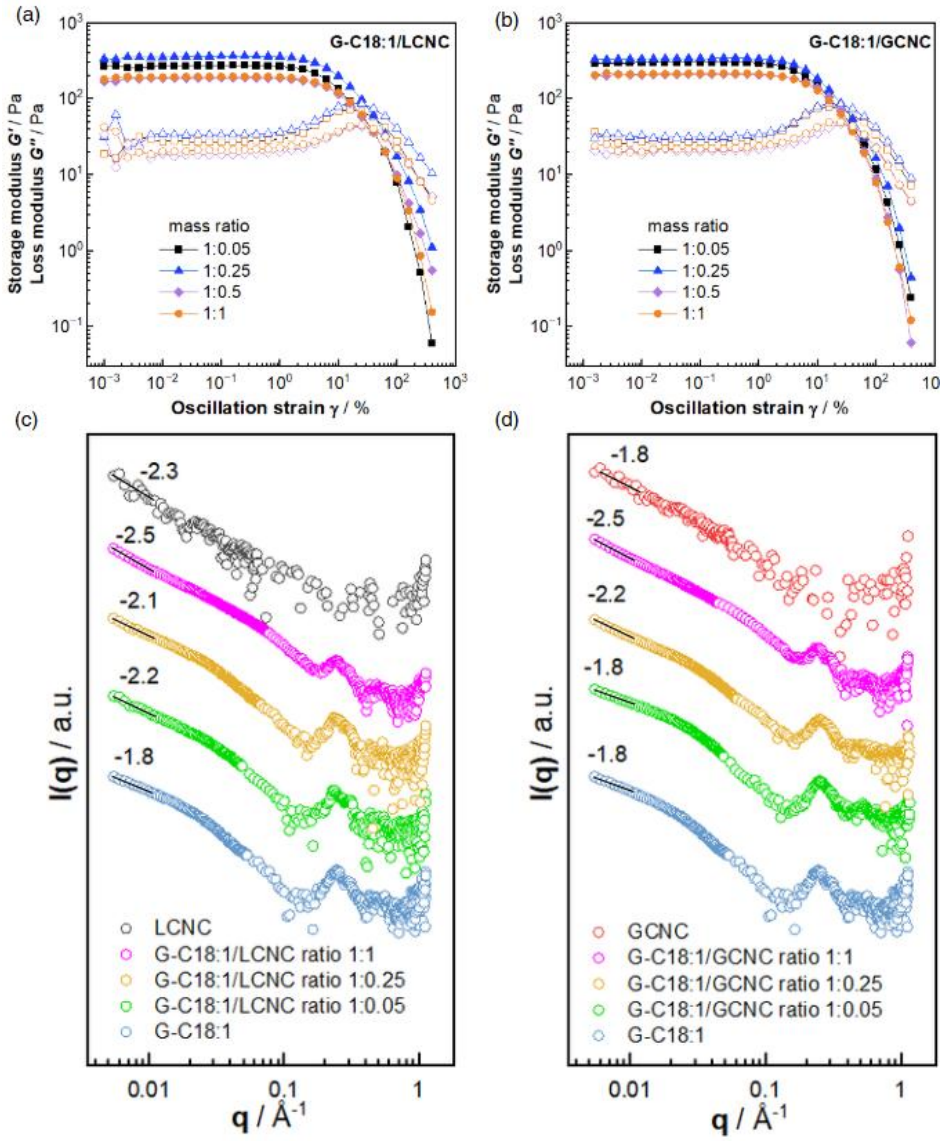

Figure 2. Oscillatory strain measurements for (a) G-C18:1/LCNC and (b) G-C18:1/GCNC gels at 1 Hz and various matrix-to-reinforcement ratios with G' being shown with closed points and G'' with open points; and (c) SAXS profiles recorded of GCNC, G-C18:1, G-C18:1/GCNC at different ratio.

SAXS : See the trend of slope following the concentration of CNC in the gel

2. *G-C18:1/HCNC*

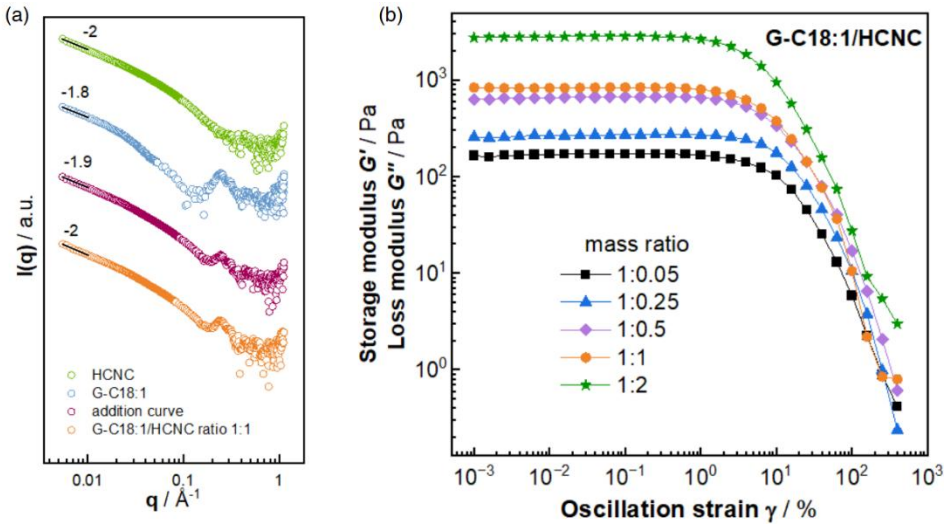

Figure 3. (a) SAXS curves of HCNC, G-C18:1, the theoretical addition curve of these two components and experimental curve of the gel; and (b) Storage modulus G' in function of oscillation strain for G-C18:1/HCNC gels various matrix-to-reinforcement ratios.

Slope of addition curve and measured curve different?

Interestingly, the G' of G-C18:1/HCNC gels are much higher than those of G-C18:1/LCNC and G-C18:1/GCNC. All the oscillatory strain measurements were reported in **Figure S4**.
-> it could due to the fact Ca2+ could also trigger the gelation of HCNC (ref) (see **Figure S5**)

➔ Explore different concentrations of Ca2+ to HCNC, G-C18:1, G-C18:1/HCNC gels

https://www.sciencedirect.com/science/article/pii/S0268005X24000730#fig1

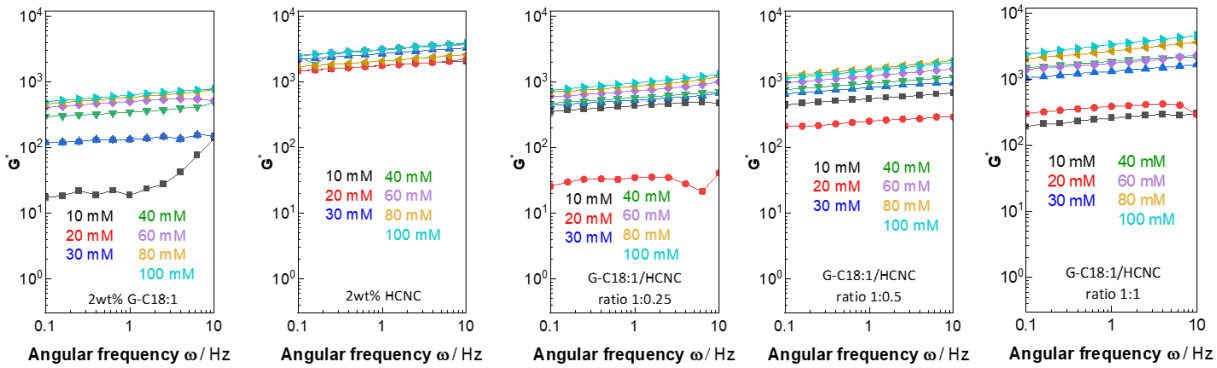

Figure 4 raport molaire Ca2+ : GC = x but how to do with the HCNC ?

X = a b c

20Mm Ca2+ always have the lowest G*. Why? = Gelation of GC first, then Ca excess go to HCNC. 30 mM -> jump to gelification of HCNC

Rheo change temperature and pH **(Figure S6)**

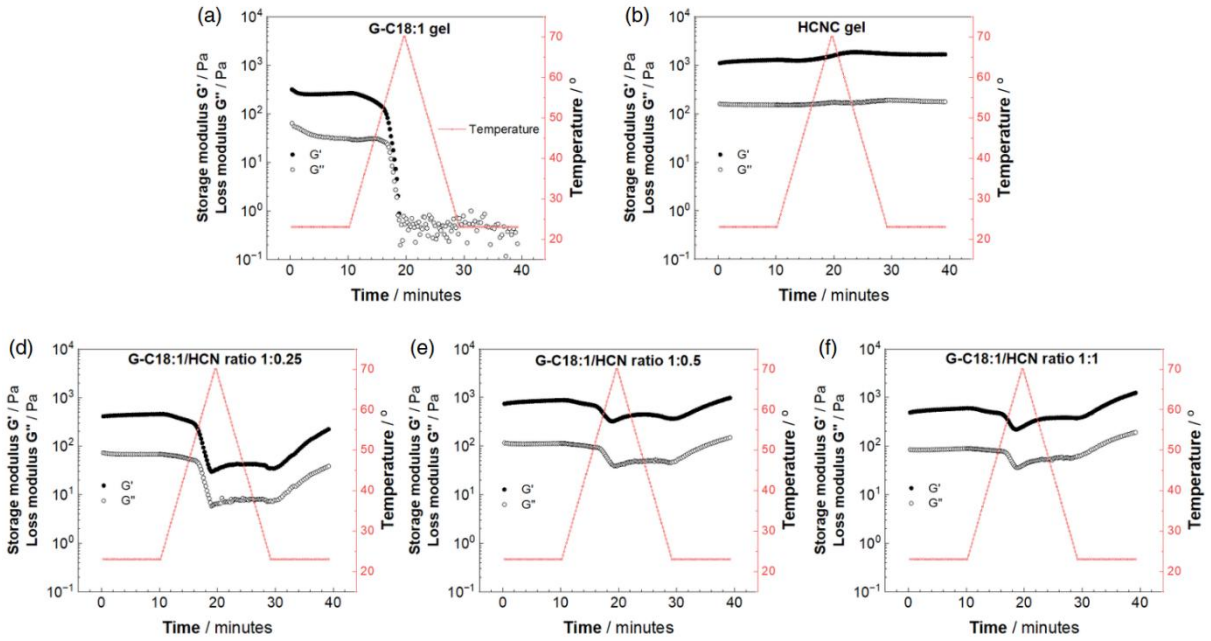

Figure 5. G-C18:1, HCNC gels and mixed gels in function of temperature

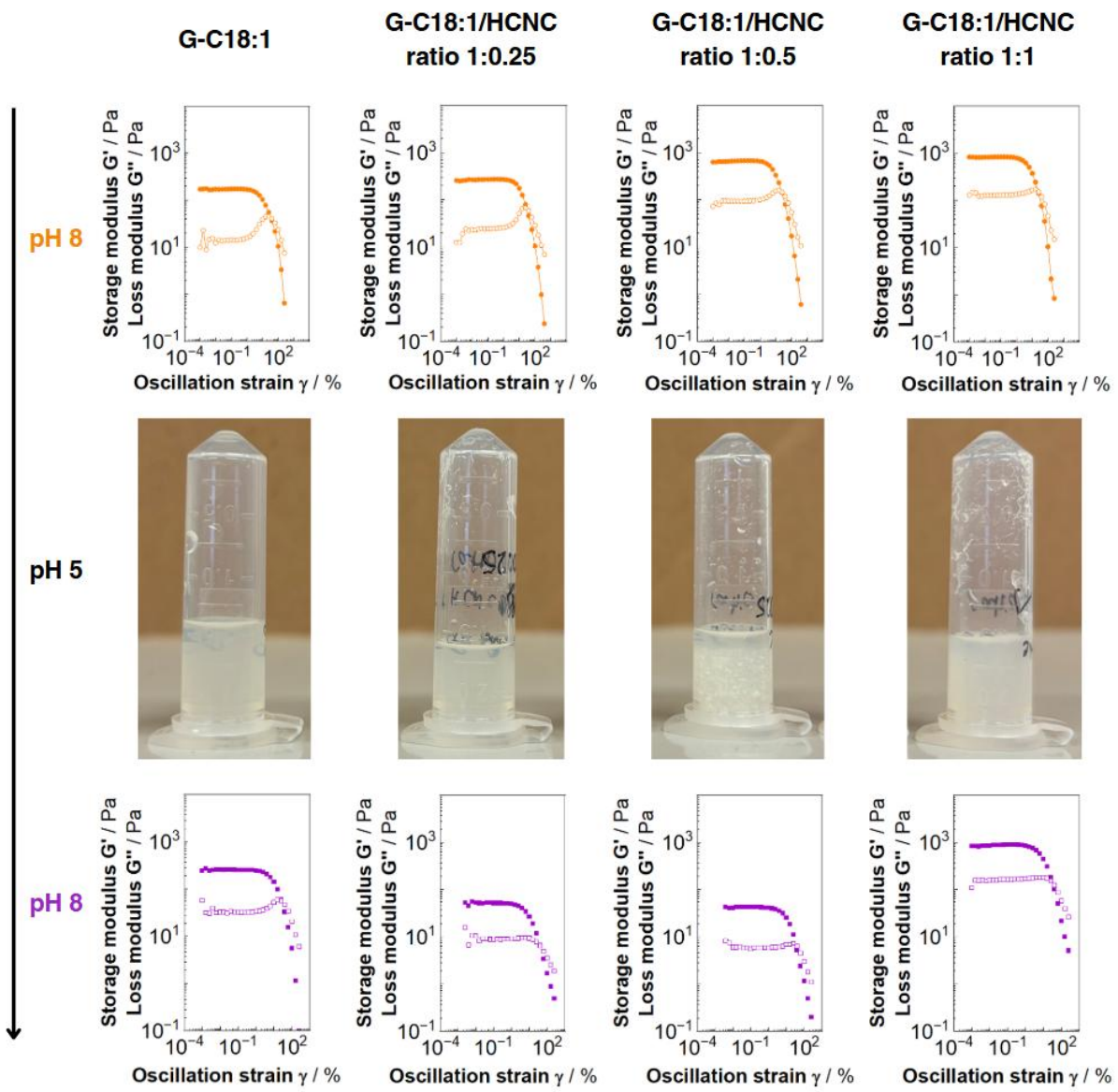
G-C18:1
G-C18:1/HCNC ratio 1:0.25
G-C18:1/HCNC ratio 1:0.5
G-C18:1/HCNC ratio 1:1
pH 8
pH 5
pH 8
Storage modulus G' / Pa
Loss modulus G'' / Pa
Oscillation strain γ / %

Figure 6

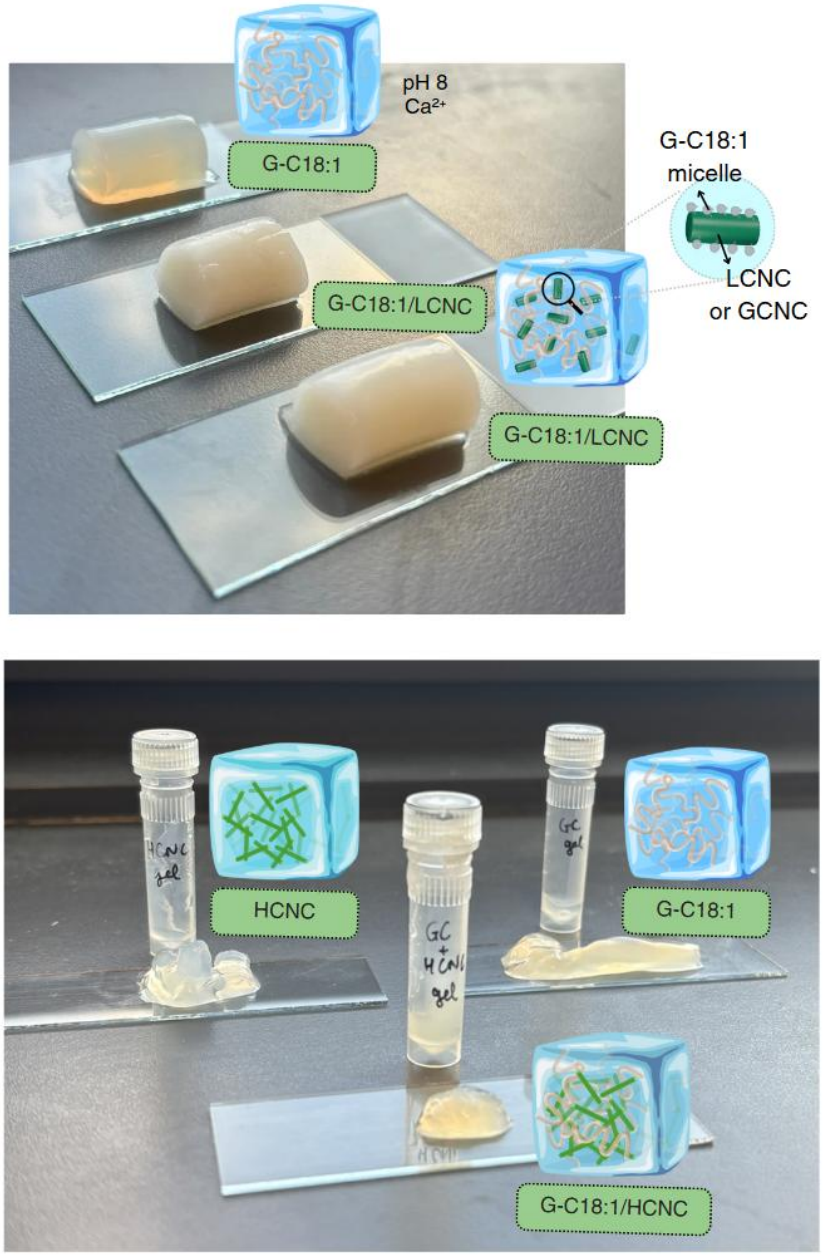

Figure 7.

3. *Rheo-SAXS of G-C18:1/CNC gels*

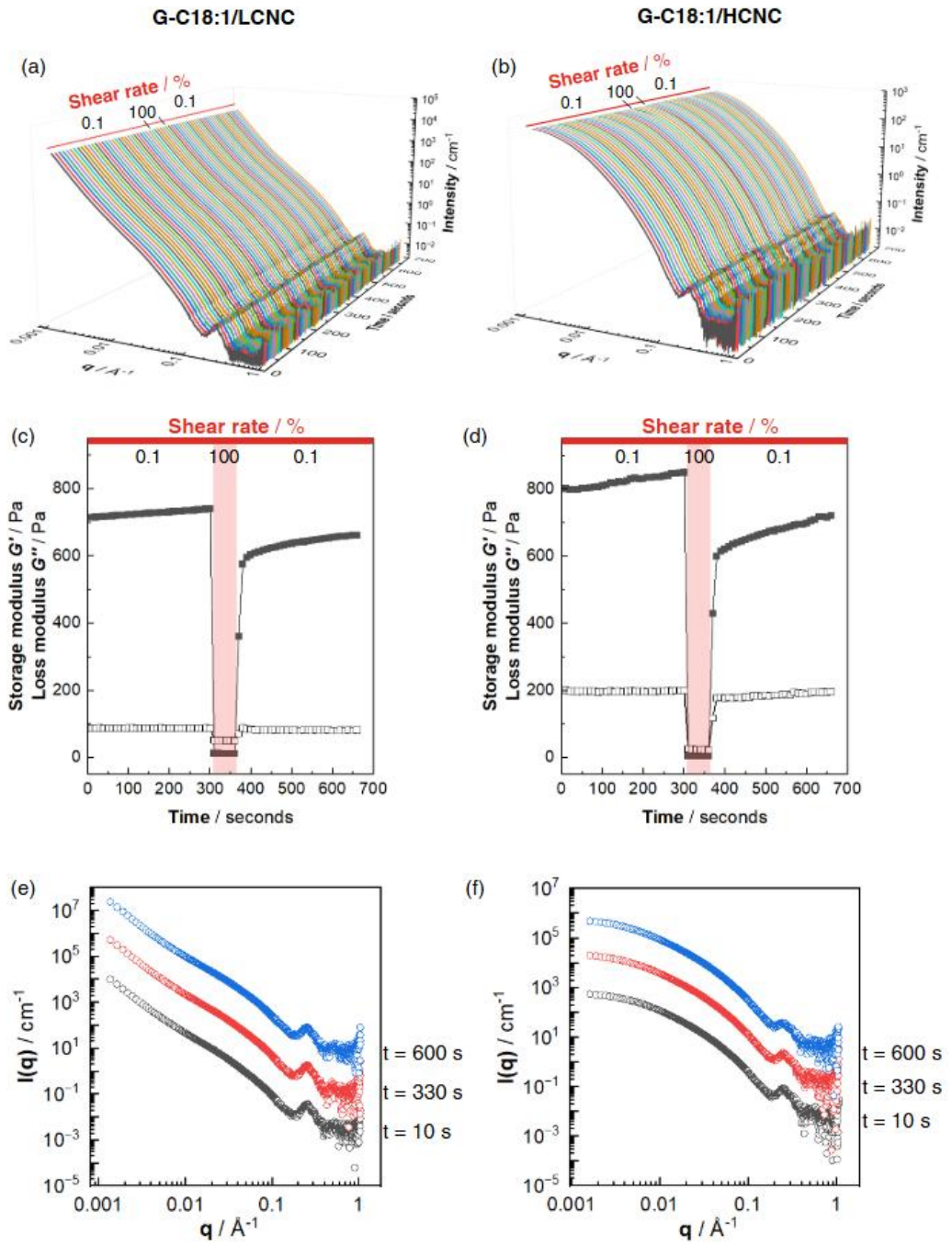

Figure 8

No change in SAXS curve for G-C18:1/Liq-HCl-CNC
But G-C18:1/H2SO4-CNC also not really different

About Rheo: same pattern, only the magnitude is different
Also G' and G'' values higher than when measured Rheo only, may due to the geometries

G-C18 :1/HCNC change shear rate **(Figure S7)**
Tangential : G-C18 :1/LCNC 1-6m & G-C18 :1/HCNC 1m **(Figure S8)**

Investigate again the G-C18:1/H2SO4-CNC, but with the shear rate increase to see the time evolution of SAXS curve.
2023-seyrig : mesh size

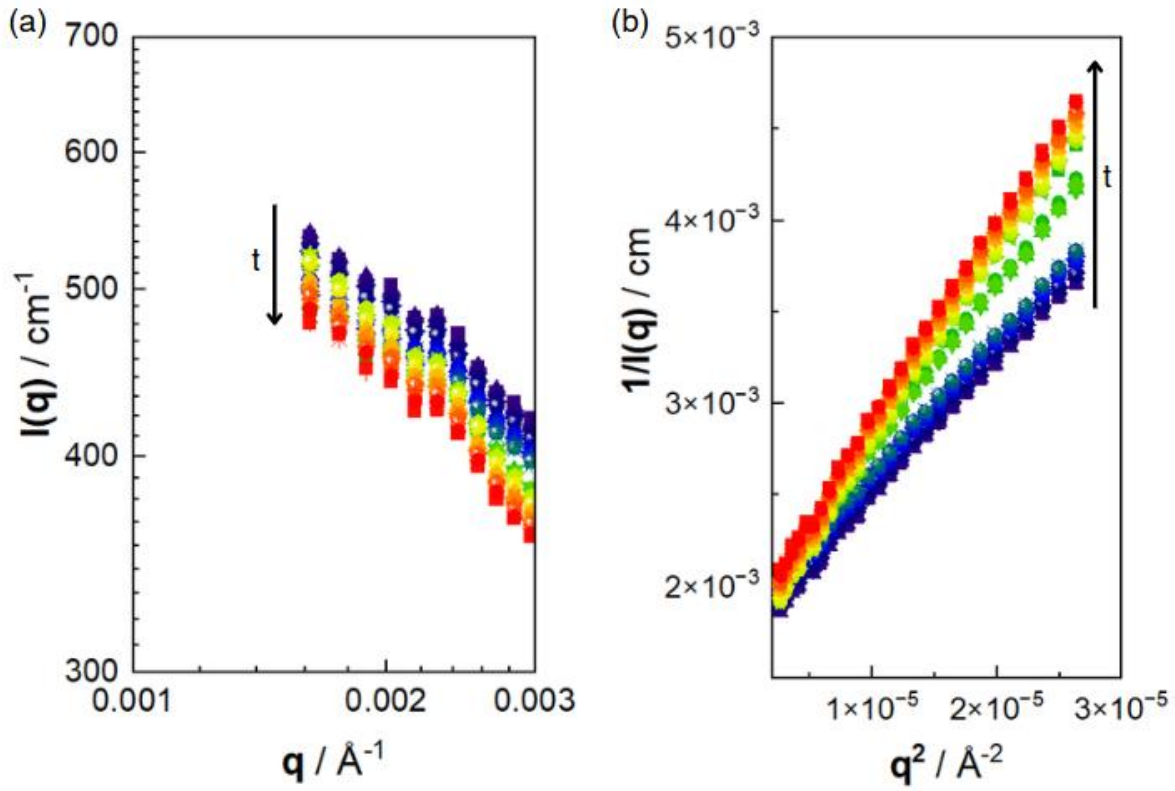

Figure 9

The Ornstein-Zernike equation is (Eq. 1)

$$I(q) = \frac{\mathrm{I}(0)}{(1+\mathrm{q}^2\xi^2)} \qquad \text{Eq. 1}$$

Which, rearranged, gives

$$I(q) = \frac{1}{I(0)} + \mathrm{q}^2 \frac{\xi^2}{I(0)} \qquad \text{Eq. 2}$$

with ξ being the mesh size of the polymer gel and $\mathrm{I}(0)$ the scattering intensity at q= 0. Plotting Eq. 3 as $\frac{1}{I(q)}$ against q^2, one could estimate ξ from the slope $\frac{\xi^2}{I(0)}$, if $\mathrm{I}(0)$ is known. However, this is unfortunately seldom the case, as the scattering plateau at q= 0 is generally not achieved for many gel and colloidal systems. As it can be easily observed, none of the SAXS profiles reported in this work reaches a plateau at q= 0, making it impossible to unambiguously quantify ξ. Despite this major drawback, one could still compare the values of the slopes in a relative fashion, supposing that $\mathrm{I}(0)$ is comparable across samples of similar structure. Figure 9 and Table 1 provide the Ornstein-Zernike plots and corresponding $\frac{\xi^2}{I(0)}$ values for the hybrid gelatin and alginate hydrogels, compared to the

controls. The values of $\frac{\xi^2}{I(0)}$ for the fiber-containing hydrogels, may them contain gelatin or alginate, are comparable to the respective controls within the incertitude of the fit. When it comes to micelle-containing hydrogels, the gelatin structure shows a smaller $\frac{\xi^2}{I(0)}$ if compared to the control. However, lacking the values of $I(0)$, it is impossible to establish a quantitative correlation between $\frac{\xi^2}{I(0)}$, the mesh size and the elastic properties of the hydrogel.

Table 1

Shear rate / %	$\overline{I(0)}$	St deviation	$\overline{\xi^2/I(0)}$	St deviation	**ξ** / Å
0.1	510	15	69.6	0.6	188.6
100	490	4	85.1	6.6	204.3
0.1	500	13	101.4	1.1	225.3

Perspective

All tan g"/g', G*, deformation point, G'-G'GC/G'GC **(table S4)**

Furthermore, for all of the gels, the values of loss factor (tan δ = G"/ G') were significantly smaller than 1, which suggested that elastic behavior dominated.

Yield and G/G

Conclusion

AUTHOR INFORMATION

Corresponding Author

E-mail: eero.kontturi@aalto.fi

E-mail: niki.baccile@sorbonne-universite.fr

Present Addresses

†If an author's address is different than the one given in the affiliation line, this information may be included here.

Author Contributions

The manuscript was written through contributions of all authors. All authors have given approval to the final version of the manuscript. ‡These authors contributed equally. (match statement to author names with a symbol)

Funding Sources

Any funds used to support the research of the manuscript should be placed here (per journal style).

Notes

Any additional relevant notes should be placed here.

ACKNOWLEDGMENT

(Word Style "TD_Acknowledgments"). Generally the last paragraph of the paper is the place to acknowledge people, organizations, and financing (you may state grant numbers and sponsors here). Follow the journal's guidelines on what to include in the Acknowledgments section.

ABBREVIATIONS

CCR2, CC chemokine receptor 2; CCL2, CC chemokine ligand 2; CCR5, CC chemokine receptor 5; TLC, thin layer chromatography.

REFERENCES

(Word Style "TF_References_Section"). References are placed at the end of the manuscript. Authors are responsible for the accuracy and completeness of all references. Examples of the recommended format for the various reference types can be found at http://pubs.acs.org/page/4authors/index.html. Detailed information on reference style can be found in *The ACS Style Guide,* available from Oxford Press.

1. Kim HJ, Jeong JH, Choi YH, Eom Y. Review on cellulose nanocrystal-reinforced polymer nanocomposites: Processing, properties, and rheology. *Korea-Australia Rheology Journal*. 2021;33(3):165-185. doi:10.1007/s13367-021-0015-z
2. Shojaeiarani J, Bajwa D, Shirzadifar A. A review on cellulose nanocrystals as promising biocompounds for the synthesis of nanocomposite hydrogels. *Carbohydr Polym*. 2019;216:247-259. doi:10.1016/j.carbpol.2019.04.033
3. Ozcelik B. Degradable hydrogel systems for biomedical applications. *Biosynthetic Polymers for Medical Applications*. Published online January 1, 2016:173-188. doi:10.1016/B978-1-78242-105-4.00007-9
4. Peppas NA, Bures P, Leobandung W, Ichikawa H. *Hydrogels in Pharmaceutical Formulations*.; 2000. www.elsevier.com/locate/ejphabio
5. Feksa LR, Troian EA, Muller CD, Viegas F, Machado AB, Rech VC. Hydrogels for biomedical applications. In: *Nanostructures for the Engineering of Cells, Tissues and Organs*. Elsevier; 2018:403-438. doi:10.1016/B978-0-12-813665-2.00011-9
6. Li M, He X, Zhao R, Shi Q, Nian Y, Hu B. Hydrogels as promising carriers for the delivery of food bioactive ingredients. *Front Nutr*. 2022;9. doi:10.3389/fnut.2022.1006520
7. Nath PC, Debnath S, Sridhar K, Inbaraj BS, Nayak PK, Sharma M. A Comprehensive Review of Food Hydrogels: Principles, Formation Mechanisms, Microstructure, and Its Applications. *Gels*. 2022;9(1):1. doi:10.3390/gels9010001
8. Draper ER, Adams DJ. Low-Molecular-Weight Gels: The State of the Art. *Chem*. 2017;3(3):390-410. doi:10.1016/j.chempr.2017.07.012
9. Adams DJ, Butler MF, Frith WJ, Kirkland M, Mullen L, Sanderson P. A new method for maintaining homogeneity during liquid–hydrogel transitions using low molecular weight hydrogelators. *Soft Matter*. 2009;5(9):1856. doi:10.1039/b901556f
10. Draper ER, Su H, Brasnett C, et al. Opening a Can of Worm(-like Micelle)s: The Effect of Temperature of Solutions of Functionalized Dipeptides. *Angewandte Chemie*. 2017;129(35):10603-10606. doi:10.1002/ange.201705604
11. Raghavan SR, Douglas JF. The conundrum of gel formation by molecular nanofibers, wormlike micelles, and filamentous proteins: gelation without cross-links? *Soft Matter*. 2012;8(33):8539. doi:10.1039/c2sm25107h
12. Yu G, Yan X, Han C, Huang F. Characterization of supramolecular gels. *Chem Soc Rev*. 2013;42(16):6697. doi:10.1039/c3cs60080g
13. Baccile N, Poirier A, Seyrig C, et al. Chameleonic amphiphile: The unique multiple self-assembly properties of a natural glycolipid in excess of water. *J Colloid Interface Sci*. 2023;630:404-415. doi:10.1016/j.jcis.2022.07.130

14. Baccile N, Selmane M, Le Griel P, et al. PH-Driven Self-Assembly of Acidic Microbial Glycolipids. *Langmuir*. 2016;32(25):6343-6359. doi:10.1021/acs.langmuir.6b00488
15. Baccile N, Cuvier AS, Prévost S, et al. Self-Assembly Mechanism of pH-Responsive Glycolipids: Micelles, Fibers, Vesicles, and Bilayers. *Langmuir*. 2016;32(42):10881-10894. doi:10.1021/acs.langmuir.6b02337
16. Poirier A, Le Griel P, Perez J, Hermida-Merino D, Pernot P, Baccile N. Metallogels from a Glycolipid Biosurfactant. *ACS Sustain Chem Eng*. 2022;10(50):16503-16515. doi:10.1021/acssuschemeng.2c01860
17. Chen M, Dong C, Penfold J, et al. Influence of Calcium Ions on Rhamnolipid and Rhamnolipid/Anionic Surfactant Adsorption and Self-Assembly. *Langmuir*. 2013;29(12):3912-3923. doi:10.1021/la400432v
18. Shen HH, Lin TW, Thomas RK, Taylor DJF, Penfold J. Surfactin Structures at Interfaces and in Solution: The Effect of pH and Cations. *J Phys Chem B*. 2011;115(15):4427-4435. doi:10.1021/jp109360h
19. Baccile N, Pedersen JS, Pehau-Arnaudet G, Van Bogaert INA. Surface charge of acidic sophorolipid micelles: effect of base and time. *Soft Matter*. 2013;9(19):4911. doi:10.1039/c3sm50160d
20. Xu H, Penfold J, Thomas RK, et al. Impact of AlCl3 on the Self-Assembly of the Anionic Surfactant Sodium Polyethylene Glycol Monoalkyl Ether Sulfate in Aqueous Solution. *Langmuir*. 2013;29(44):13359-13366. doi:10.1021/la403278x
21. Alargova RG, Petkov JT, Petsev DN. Micellization and interfacial properties of alkyloxyethylene sulfate surfactants in the presence of multivalent counterions. *J Colloid Interface Sci*. 2003;261(1):1-11. doi:10.1016/S0021-9797(03)00027-4
22. Alargova RG, Danov KD, Kralchevsky PA, Broze G, Mehreteab A. Growth of Giant Rodlike Micelles of Ionic Surfactant in the Presence of Al^{3+} Counterions. *Langmuir*. 1998;14(15):4036-4049. doi:10.1021/la970684x
23. Srinivasan V, Blankschtein D. Effect of Counterion Binding on Micellar Solution Behavior: 2. Prediction of Micellar Solution Properties of Ionic Surfactant−Electrolyte Systems. *Langmuir*. 2003;19(23):9946-9961. doi:10.1021/la030070u
24. Angelescu D, Caldararu H, Khan A. Some observations on the effect of the trivalent counterion Al3+ to the self-assembly of sodium dodecyl sulphate in water. *Colloids Surf A Physicochem Eng Asp*. 2004;245(1-3):49-60. doi:10.1016/j.colsurfa.2004.01.040
25. Penfold J, Thomas RK, Dong CC, et al. Equilibrium Surface Adsorption Behavior in Complex Anionic/Nonionic Surfactant Mixtures. *Langmuir*. 2007;23(20):10140-10149. doi:10.1021/la701151m
26. Eichhorn SJ, Dufresne A, Aranguren M, et al. Review: current international research into cellulose nanofibres and nanocomposites. *J Mater Sci*. 2010;45(1):1-33. doi:10.1007/s10853-009-3874-0
27. Moon RJ, Martini A, Nairn J, Simonsen J, Youngblood J. *Cellulose Nanomaterials Review: Structure, Properties and Nanocomposites*. Vol 40.; 2011. doi:10.1039/c0cs00108b
28. Habibi Y, Lucia LA, Rojas OJ. Cellulose nanocrystals: Chemistry, self-assembly, and applications. *Chem Rev*. 2010;110(6):3479-3500. doi:10.1021/cr900339w
29. Thomas B, Raj MC, Athira BK, et al. Nanocellulose, a Versatile Green Platform: From Biosources to Materials and Their Applications. *Chem Rev*. 2018;118(24):11575-11625. doi:10.1021/acs.chemrev.7b00627

30. Mariano M, El Kissi N, Dufresne A. Cellulose nanocrystals and related nanocomposites: Review of some properties and challenges. *J Polym Sci B Polym Phys*. 2014;52(12):791-806. doi:10.1002/polb.23490
31. Klemm D, Heublein B, Fink HP, Bohn A. Cellulose: Fascinating biopolymer and sustainable raw material. *Angewandte Chemie - International Edition*. 2005;44(22):3358-3393. doi:10.1002/anie.200460587
32. Klemm D, Kramer F, Moritz S, et al. Nanocelluloses: A New Family of Nature-Based Materials. *Angewandte Chemie International Edition*. 2011;50(24):5438-5466. doi:10.1002/anie.201001273
33. Rana AK, Frollini E, Thakur VK. Cellulose nanocrystals: Pretreatments, preparation strategies, and surface functionalization. *Int J Biol Macromol*. 2021;182:1554-1581. doi:10.1016/j.ijbiomac.2021.05.119
34. Nagarajan KJ, Ramanujam NR, Sanjay MR, et al. *A Comprehensive Review on Cellulose Nanocrystals and Cellulose Nanofibers: Pretreatment, Preparation, and Characterization*. Vol 42.; 2021. doi:10.1002/pc.25929
35. Mohd Amin KN, Annamalai PK, Morrow IC, Martin D. Production of cellulose nanocrystals via a scalable mechanical method. *RSC Adv*. 2015;5(70):57133-57140. doi:10.1039/C5RA06862B
36. Vanderfleet OM, Cranston ED. Production routes to tailor the performance of cellulose nanocrystals. *Nat Rev Mater*. 2020;6(2):124-144. doi:10.1038/s41578-020-00239-y
37. Kontturi E. Preparation of Cellulose Nanocrystals Background, Conventions and New Developments. In: *Nanocellulose and Sustainability Production, Properties, Applications, and Case Studies*. Vol Chapter 3. ; 2018:27-40.
38. Xie H, Du H, Yang X, Si C. Recent Strategies in Preparation of Cellulose Nanocrystals and Cellulose Nanofibrils Derived from Raw Cellulose Materials. *Int J Polym Sci*. 2018;2018:1-25. doi:10.1155/2018/7923068
39. Eichhorn SJ. Cellulose nanowhiskers: Promising materials for advanced applications. *Soft Matter*. 2011;7(2):303-315. doi:10.1039/c0sm00142b
40. Moon RJ, Martini A, Nairn J, Simonsen J, Youngblood J. Cellulose nanomaterials review: structure, properties and nanocomposites. *Chem Soc Rev*. 2011;40(7):3941. doi:10.1039/c0cs00108b
41. Natarajan B, Gilman JW. Bioinspired Bouligand cellulose nanocrystal composites: a review of mechanical properties. *Philosophical Transactions of the Royal Society A: Mathematical, Physical and Engineering Sciences*. 2018;376(2112):20170050. doi:10.1098/rsta.2017.0050
42. Lin N, Huang J, Dufresne A. Preparation, properties and applications of polysaccharide nanocrystals in advanced functional nanomaterials: a review. *Nanoscale*. 2012;4(11):3274. doi:10.1039/c2nr30260h
43. Huang S, Zhou L, Li MC, Wu Q, Zhou D. Cellulose Nanocrystals (CNCs) from Corn Stalk: Activation Energy Analysis. *Materials*. 2017;10(1):80. doi:10.3390/ma10010080
44. Domingues RMA, Gomes ME, Reis RL. The Potential of Cellulose Nanocrystals in Tissue Engineering Strategies. *Biomacromolecules*. 2014;15(7):2327-2346. doi:10.1021/bm500524s
45. Amin KNM, Hosseinmardi A, Martin DJ, Annamalai PK. A mixed acid methodology to produce thermally stable cellulose nanocrystal at high yield using phosphoric acid. *Journal of Bioresources and Bioproducts*. 2022;7(2):99-108. doi:10.1016/j.jobab.2021.12.002

46. Cheng M, Qin Z, Hu J, et al. Facile and rapid one–step extraction of carboxylated cellulose nanocrystals by H2SO4/HNO3 mixed acid hydrolysis. *Carbohydr Polym*. 2020;231:115701. doi:10.1016/j.carbpol.2019.115701
47. Cheng M, Qin Z, Chen Y, Hu S, Ren Z, Zhu M. Efficient Extraction of Cellulose Nanocrystals through Hydrochloric Acid Hydrolysis Catalyzed by Inorganic Chlorides under Hydrothermal Conditions. *ACS Sustain Chem Eng*. 2017;5(6):4656-4664. doi:10.1021/acssuschemeng.6b03194
48. Sofla MRK, Brown RJ, Tsuzuki T, Rainey TJ. A comparison of cellulose nanocrystals and cellulose nanofibres extracted from bagasse using acid and ball milling methods. *Advances in Natural Sciences: Nanoscience and Nanotechnology*. 2016;7(3):035004. doi:10.1088/2043-6262/7/3/035004
49. Tang Y, Yang H, Vignolini S. Recent Progress in Production Methods for Cellulose Nanocrystals: Leading to More Sustainable Processes. *Adv Sustain Syst*. 2022;6(3). doi:10.1002/adsu.202100100
50. Lorenz M, Sattler S, Reza M, Bismarck A, Kontturi E. Cellulose nanocrystals by acid vapour: Towards more effortless isolation of cellulose nanocrystals. *Faraday Discuss*. 2017;202:315-330. doi:10.1039/c7fd00053g
51. Kontturi E, Meriluoto A, Penttilä PA, et al. Degradation and Crystallization of Cellulose in Hydrogen Chloride Vapor for High-Yield Isolation of Cellulose Nanocrystals. *Angewandte Chemie*. 2016;55(46):14455 –14458. doi:10.1002/anie.201606626
52. Pääkkönen T, Spiliopoulos P, Knuts A, et al. From vapour to gas: Optimising cellulose degradation with gaseous HCl. *React Chem Eng*. 2018;3(3):312-318. doi:10.1039/c7re00215g
53. Klemm D, Kramer F, Moritz S, et al. Nanocelluloses: A new family of nature-based materials. *Angewandte Chemie - International Edition*. 2011;50(24):5438-5466. doi:10.1002/anie.201001273
54. Eyley S, Thielemans W. Surface modification of cellulose nanocrystals. *Nanoscale*. 2014;6(14):7764-7779. doi:10.1039/c4nr01756k
55. Abushammala H, Mao J. A Review of the Surface Modification of Cellulose. *Molecules*. 2019;24(Figure 2):1-18.
56. Fraschini C, Chauve G, Bouchard J. TEMPO-mediated surface oxidation of cellulose nanocrystals (CNCs). *Cellulose*. 2017;24(7):2775-2790. doi:10.1007/s10570-017-1319-5
57. Cao X, Ding B, Yu J, Al-Deyab SS. Cellulose nanowhiskers extracted from TEMPO-oxidized jute fibers. *Carbohydr Polym*. 2012;90(2):1075-1080. doi:10.1016/j.carbpol.2012.06.046
58. Cohen N, Ochbaum G, Levi-Kalisman Y, Bitton R, Yerushalmi-Rozen R. Polymer-Induced Modification of Cellulose Nanocrystal Assemblies in Aqueous Suspensions. *ACS Appl Polym Mater*. 2020;2(2):732-740. doi:10.1021/acsapm.9b01048
59. Wang Y, Wang X, Xie Y, Zhang K. Functional nanomaterials through esterification of cellulose: a review of chemistry and application. *Cellulose*. 2018;25(7):3703-3731. doi:10.1007/s10570-018-1830-3
60. Li D, Henschen J, Ek M. Esterification and hydrolysis of cellulose using oxalic acid dihydrate in a solvent-free reaction suitable for preparation of surface-functionalised cellulose nanocrystals with high yield. *Green Chemistry*. 2017;19(23):5564-5567. doi:10.1039/c7gc02489d
61. Berlioz S, Molina-Boisseau S, Nishiyama Y, Heux L. Gas-Phase Surface Esterification of Cellulose Microfibrils and Whiskers. *Biomacromolecules*. 2009;10(8):2144-2151. doi:10.1021/bm900319k

62. Wu Z, Xu J, Gong J, Li J, Mo L. Preparation, characterization and acetylation of cellulose nanocrystal allomorphs. *Cellulose*. 2018;25(9):4905-4918. doi:10.1007/s10570-018-1937-6
63. Sass J francois, Chanzy H. *Ultrastructural Aspects of the Acetylation of Cellulose*. Vol 2.; 1995.
64. Araki J, Wada M, Kuga S. Steric Stabilization of a Cellulose Microcrystal Suspension by Poly(ethylene glycol) Grafting. *Langmuir*. 2000;17(1):21-27. doi:10.1021/la001070m
65. H. M. Kan K, Li J, Wijesekera K, D. Cranston E. Polymer-Grafted Cellulose Nanocrystals as pH-Responsive Reversible Flocculants. *Biomacromolecules*. 2013;14(9):3130-3139. doi:10.1021/bm400752k
66. Laitinen O, Hartmann R, Sirviö JA, et al. Alkyl aminated nanocelluloses in selective flotation of aluminium oxide and quartz. *Chem Eng Sci*. 2016;144:260-266. doi:10.1016/J.CES.2016.01.052
67. Chen Y, Liu Y, Xia Y, et al. Electric Field-Induced Assembly and Alignment of Silver-Coated Cellulose for Polymer Composite Films with Enhanced Dielectric Permittivity and Anisotropic Light Transmission. *ACS Applied Materials & Interfaces*. 2020;12(21):24242-24249. doi:10.1021/acsami.0c03086
68. Majoinen J, Walther A, R. McKee J, et al. Polyelectrolyte Brushes Grafted from Cellulose Nanocrystals Using Cu-Mediated Surface-Initiated Controlled Radical Polymerization. *Biomacromolecules*. 2011;12(8):2997-3006. doi:10.1021/bm200613y
69. Majoinen J, Gustavsson L, Wani O, et al. Controlling the Nematic Liquid Crystallinity of Cellulose Nanocrystals with an Alcohol Ethoxy Sulfonate Surfactant. *Biomacromolecules*. 2024;0(0). doi:10.1021/acs.biomac.3c01375
70. Chi K, Catchmark JM. Enhanced dispersion and interface compatibilization of crystalline nanocellulose in polylactide by surfactant adsorption. *Cellulose*. 2017;24(11):4845-4860. doi:10.1007/s10570-017-1479-3
71. Kaboorani A, Riedl B. Surface modification of cellulose nanocrystals (CNC) by a cationic surfactant. *Ind Crops Prod*. 2015;65:45-55. doi:10.1016/J.INDCROP.2014.11.027
72. Tardy BL, Yokota S, Ago M, et al. Nanocellulose–surfactant interactions. *Curr Opin Colloid Interface Sci*. 2017;29:57-67. doi:10.1016/j.cocis.2017.02.004
73. Trache D, Tarchoun AF, Derradji M, et al. *Nanocellulose: From Fundamentals to Advanced Applications*. Vol 8.; 2020. doi:10.3389/fchem.2020.00392
74. Yang J, Han CR, Duan JF, et al. Synthesis and characterization of mechanically flexible and tough cellulose nanocrystals–polyacrylamide nanocomposite hydrogels. *Cellulose*. 2013;20(1):227-237. doi:10.1007/s10570-012-9841-y
75. Spagnol C, Rodrigues FHA, Neto AGVC, et al. Nanocomposites based on poly(acrylamide-co-acrylate) and cellulose nanowhiskers. *Eur Polym J*. 2012;48(3):454-463. doi:10.1016/j.eurpolymj.2011.12.005
76. Martínez DG, Stading M, Hermansson AM. Viscoelasticity and microstructure of a hierarchical soft composite based on nano-cellulose and κ-carrageenan. *Rheol Acta*. 2013;52(10-12):823-831. doi:10.1007/s00397-013-0721-7
77. Dash R, Foston M, Ragauskas AJ. Improving the mechanical and thermal properties of gelatin hydrogels cross-linked by cellulose nanowhiskers. *Carbohydr Polym*. 2013;91(2):638-645. doi:10.1016/j.carbpol.2012.08.080
78. Abitbol T, Johnstone T, Quinn TM, Gray DG. Reinforcement with cellulose nanocrystals of poly(vinyl alcohol) hydrogels prepared by cyclic freezing and thawing. *Soft Matter*. 2011;7(6):2373. doi:10.1039/c0sm01172j

79. Gonzalez JS, Ludueña LN, Ponce A, Alvarez VA. Poly(vinyl alcohol)/cellulose nanowhiskers nanocomposite hydrogels for potential wound dressings. *Materials Science and Engineering: C*. 2014;34:54-61. doi:10.1016/j.msec.2013.10.006
80. McKee JR, Appel EA, Seitsonen J, Kontturi E, Scherman OA, Ikkala O. Healable, Stable and Stiff Hydrogels: Combining Conflicting Properties Using Dynamic and Selective Three-Component Recognition with Reinforcing Cellulose Nanorods. *Adv Funct Mater*. 2014;24(18):2706-2713. doi:10.1002/adfm.201303699
81. Spagnol C, Rodrigues FHA, Neto AGVC, et al. Nanocomposites based on poly(acrylamide-co-acrylate) and cellulose nanowhiskers. *Eur Polym J*. 2012;48(3):454-463. doi:10.1016/j.eurpolymj.2011.12.005
82. Yang J, Han CR, Zhang XM, Xu F, Sun RC. Cellulose Nanocrystals Mechanical Reinforcement in Composite Hydrogels with Multiple Cross-Links: Correlations between Dissipation Properties and Deformation Mechanisms. *Macromolecules*. 2014;47(12):4077-4086. doi:10.1021/ma500729q
83. Yang J, Zhang XM, Xu F. Design of Cellulose Nanocrystals Template-Assisted Composite Hydrogels: Insights from Static to Dynamic Alignment. *Macromolecules*. 2015;48(4):1231-1239. doi:10.1021/ma5026175
84. Palaganas NB, Mangadlao JD, de Leon ACC, et al. 3D Printing of Photocurable Cellulose Nanocrystal Composite for Fabrication of Complex Architectures via Stereolithography. *ACS Appl Mater Interfaces*. 2017;9(39):34314-34324. doi:10.1021/acsami.7b09223
85. Wang J, Chiappone A, Roppolo I, et al. All-in-One Cellulose Nanocrystals for 3D Printing of Nanocomposite Hydrogels. *Angewandte Chemie International Edition*. 2018;57(9):2353-2356. doi:10.1002/anie.201710951
86. Abdollahi M, Alboofetileh M, Rezaei M, Behrooz R. Comparing physico-mechanical and thermal properties of alginate nanocomposite films reinforced with organic and/or inorganic nanofillers. *Food Hydrocoll*. 2013;32(2):416-424. doi:10.1016/j.foodhyd.2013.02.006
87. Khan A, Khan RA, Salmieri S, et al. Mechanical and barrier properties of nanocrystalline cellulose reinforced chitosan based nanocomposite films. *Carbohydr Polym*. 2012;90(4):1601-1608. doi:10.1016/j.carbpol.2012.07.037
88. Yang X, Bakaic E, Hoare T, Cranston ED. Injectable Polysaccharide Hydrogels Reinforced with Cellulose Nanocrystals: Morphology, Rheology, Degradation, and Cytotoxicity. *Biomacromolecules*. 2013;14(12):4447-4455. doi:10.1021/bm401364z
89. Ben Azouz K, Ramires EC, Van den Fonteyne W, El Kissi N, Dufresne A. Simple Method for the Melt Extrusion of a Cellulose Nanocrystal Reinforced Hydrophobic Polymer. *ACS Macro Lett*. 2012;1(1):236-240. doi:10.1021/mz2001737
90. Fox J, Wie JJ, Greenland BW, et al. High-Strength, Healable, Supramolecular Polymer Nanocomposites. *J Am Chem Soc*. 2012;134(11):5362-5368. doi:10.1021/ja300050x
91. Yang J, Han CR, Duan JF, et al. Studies on the properties and formation mechanism of flexible nanocomposite hydrogels from cellulose nanocrystals and poly(acrylic acid). *J Mater Chem*. 2012;22(42):22467. doi:10.1039/c2jm35498e
92. Yang J, Han C rui, Xu F, Sun R cang. Simple approach to reinforce hydrogels with cellulose nanocrystals. *Nanoscale*. 2014;6(11):5934. doi:10.1039/c4nr01214c
93. Tang J, Javaid MU, Pan C, Yu G, Berry RM, Tam KC. Self-healing stimuli-responsive cellulose nanocrystal hydrogels. *Carbohydr Polym*. 2020;229:115486. doi:10.1016/j.carbpol.2019.115486

94. Du H, Liu W, Zhang M, Si C, Zhang X, Li B. Cellulose nanocrystals and cellulose nanofibrils based hydrogels for biomedical applications. *Carbohydr Polym*. 2019;209:130-144. doi:10.1016/j.carbpol.2019.01.020
95. Lin N, Dufresne A. Nanocellulose in biomedicine: Current status and future prospect. *Eur Polym J*. 2014;59:302-325. doi:10.1016/j.eurpolymj.2014.07.025
96. Abitbol T, Rivkin A, Cao Y, et al. Nanocellulose, a tiny fiber with huge applications. *Curr Opin Biotechnol*. 2016;39:76-88. doi:10.1016/j.copbio.2016.01.002
97. Karen M. J. Saerens*, Jinxin Zhang, Lien Saey INAVB and WS. Cloning and functional characterizationof the UDP-glucosyltransferase UgtB1 involvedin sophorolipid production byCandida bombicolaand creation of a glucolipid-producing yeast strain. *Yeast*. 2011;28(January):279-292. doi:10.1002/yea
98. D. Klemm BPTHUHWW. *Comprehensive Cellulose Chemistry*. Vol Vol. 1. Wiley-VCH, Weinheim; 1998.

Interpenetrated hydrogels composed of cellulose nanocrystals and biosurfactants

Thuy-Linh Phi [a,b] *, Niki Baccile* [a,*]*, Eero Kontturi* [b,*]

[a] Sorbonne Université, Centre National de la Recherche Scientifique, Laboratoire de Chimie de la Matière Condensée de Paris, LCMCP, F-75005 Paris, France

[b] Department of Bioproducts and Biosystems, School of Chemical Engineering, Aalto University, P.O. Box 16300, 00076 Aalto, Finland

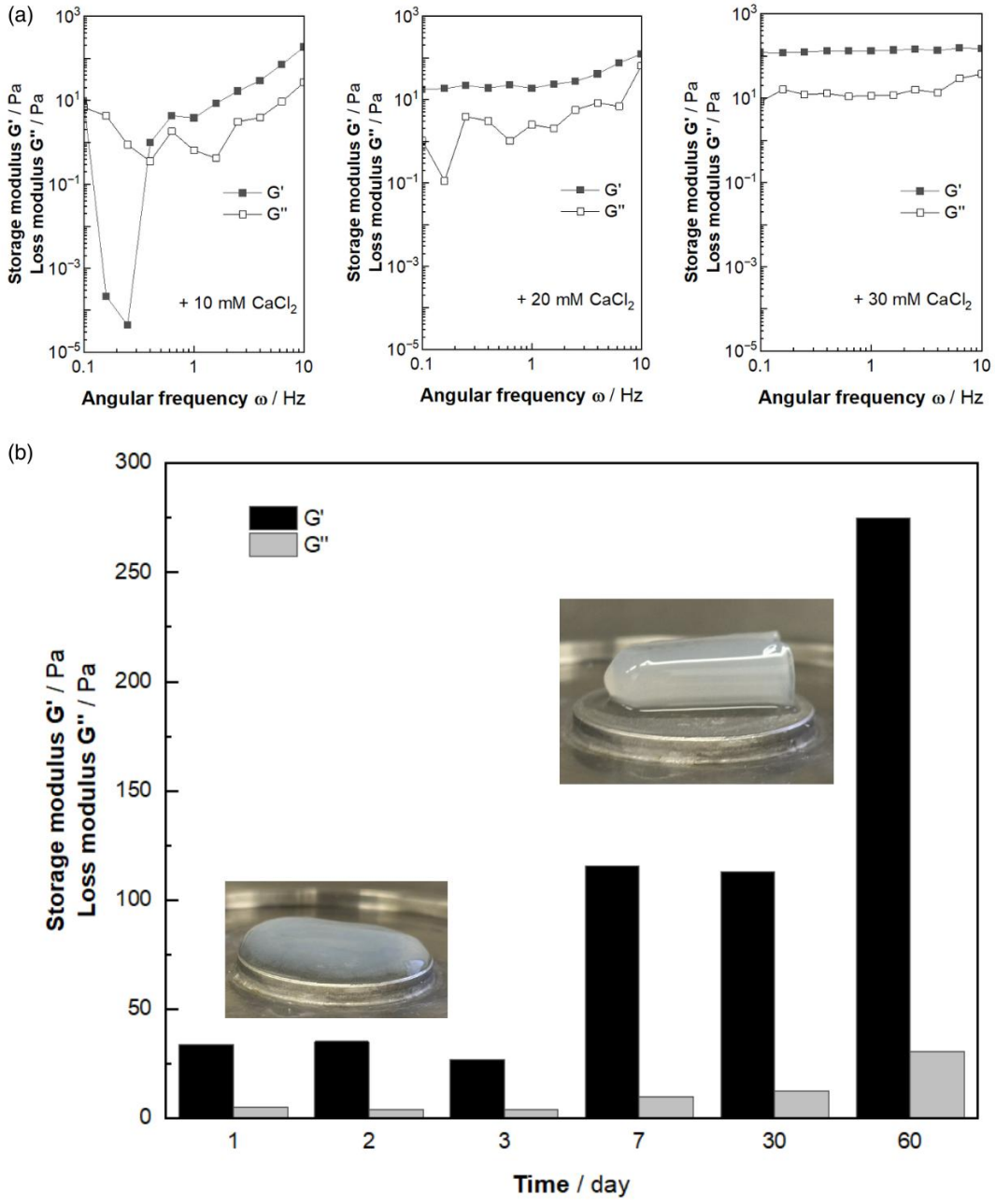

Figure S1. (a) Typical frequency sweep storage (full symbols) and loss (empty symbols) moduli for 2 wt% G-C18:1 with the addition of different concentrations of $CaCl_2$ 1M; and (b) Time-dependent of the storage and loss moduli (f= 1 Hz, γ= 0.1 %) of G-C18:1 gels triggered by 27 µL $CaCl_2$ tracked for a period of 2 months.

Figure S2. The G-C18:1 solution is prone to aggregation over time, leading to inconsistencies in gel properties. Sonication prior to each use effectively disperses aggregates, ensuring consistent gel quality.

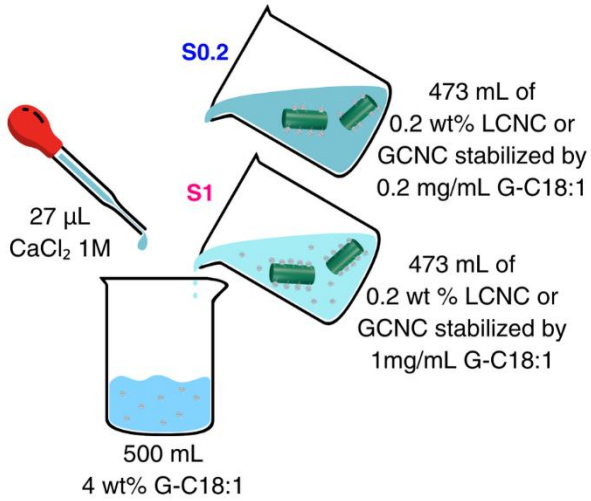

Figure S3. The illustration of the GC/LCNC and GC/GCNC preparations.

Table S1. Storage (G') and loss (G'') moduli (Pa) were measured for GC/LCNC (S0.2 and S1) gels at various LCNC concentrations after 2 and 7 days.

GC/LCNC ratio	1:0.05		1:0.25		1:0.5		1:1	
	G'	**G''**	**G'**	**G''**	**G'**	**G''**	**G'**	**G''**
S0.2 day 2	118.39	13.55	129.75	17.15				
S0.2 day 7	232.78	22.29	316.37	29.80	186.86	18.49	194.39	21.23
S1 day 2	39.62	4.49	61.42	7.42	112.09	15.77	57.48	8.53
S1 day 7	177.27	16.87	215.52	19.16	150.43	19.64	94.73	14.54

Table S2. Storage (G') and loss (G'') moduli (Pa) were measured for GC/GCNC (S0.2 and S1) at various GCNC concentrations after 2 and 7 days.

GC/ GCNC ratio	1:0.05		1:0.25		1:0.5		1:1	
	G'	**G''**	**G'**	**G''**	**G'**	**G''**	**G'**	**G''**
S0.2 day 2	141.97	15.52	156.79	17.47	90.97	12.68	78.26	10.52
S0.2 day 7	299.18	27.35	321.68	29.40	351.42	35.53	376.94	40.22
S1 day 2	27.26	4.06	51.80	6.42	90.97	12.68	78.26	10.52
S1 day 7	189.43	15.41	208.77	20.54	351.42	35.53	376.94	40.22

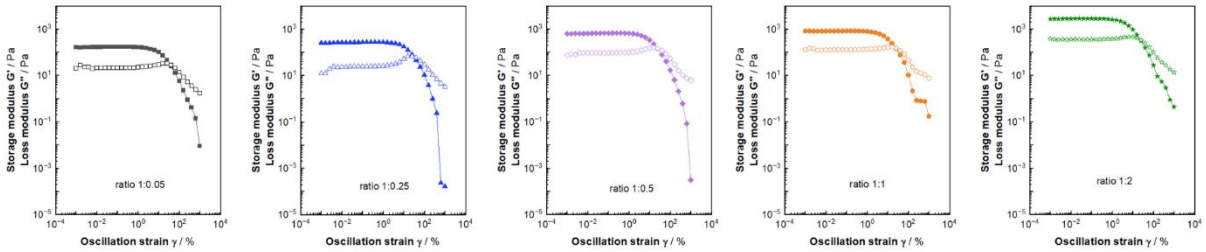

Figure S4. Oscillatory strain measurements for G-C18:1/HCNC gels at 1 Hz and various matrix-to-reinforcement ratios with G' being shown with closed points and G' ' with open points.

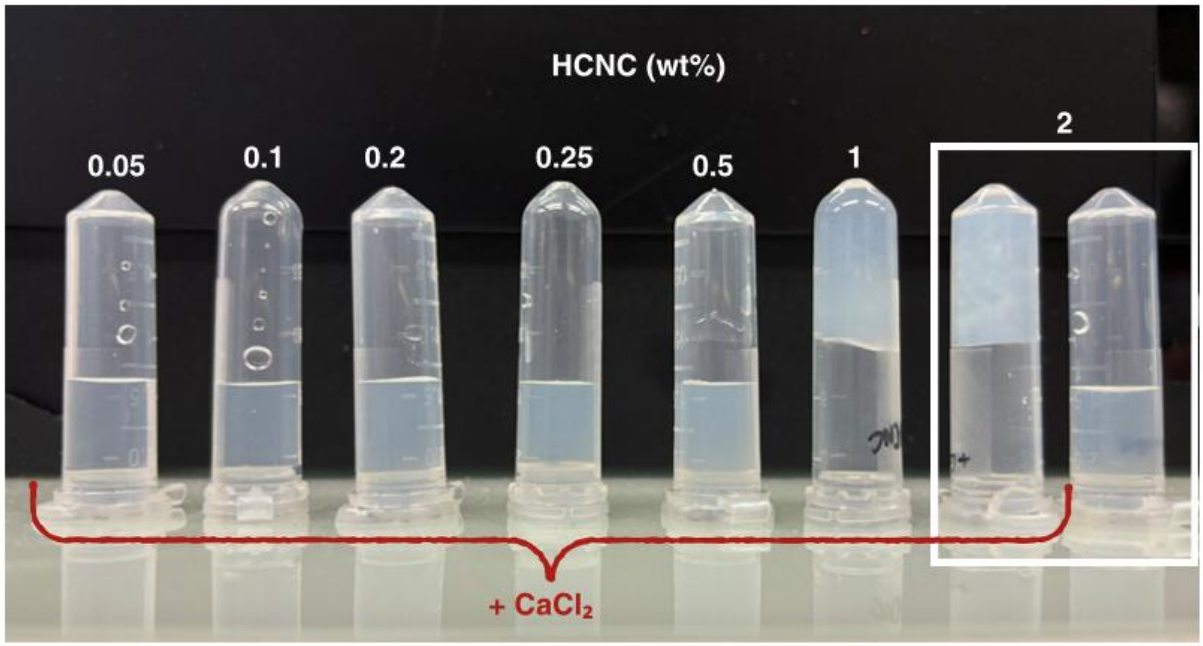

Figure S5.

Table S 3

GC/HCNC	ratio									
	1:0.05		1:0.25		1:0.5		1:1		1:2	
	G'	G''	G'	G''	G'	G''	G'	G''	G'	G''
Day 2	68.25	7.62	101.44	11.18	340.08	62.50	479.73	91.49	2311.14	380.40
Day 7	140.28	13.57	265.92	25.18	663.60	94.57	828.06	128.77	2793.49	362.72

ratio

		1:0.05	1:0.25	1:0.5	1:1	1:2
GC/ LCNC	**tan δ**	0.095	0.094	0.098	0.109	
	|G*|	233.85	317.77	187.78	195.54	
	Deformation point (%)	21.6	29.9	36.8	36.7	
	$(G'-G'_{GC})/G'_{GC}$	1.02	1.75	0.62	0.69	
GC/ GCNC	**tan δ**	0.091	0.091	0.101	0.106	
	|G*|	300.43	323.03	353.21	379.08	
	Deformation point (%)	22.9	26.3	37.2	32.8	
	$(G'-G'_{GC})/G'_{GC}$	1.60	1.79	2.05	2.27	
GC/ HCNC	**tan δ**	0.096	0.094	0.142	0.155	0.129
	|G*|	140.94	267.11	670.30	838.02	2816.94
	Deformation point (%)	34.9	30.5	24.7	23.3	22.6
	$(G'-G'_{GC})/G'_{GC}$	0.21	1.31	4.77	6.20	23.29

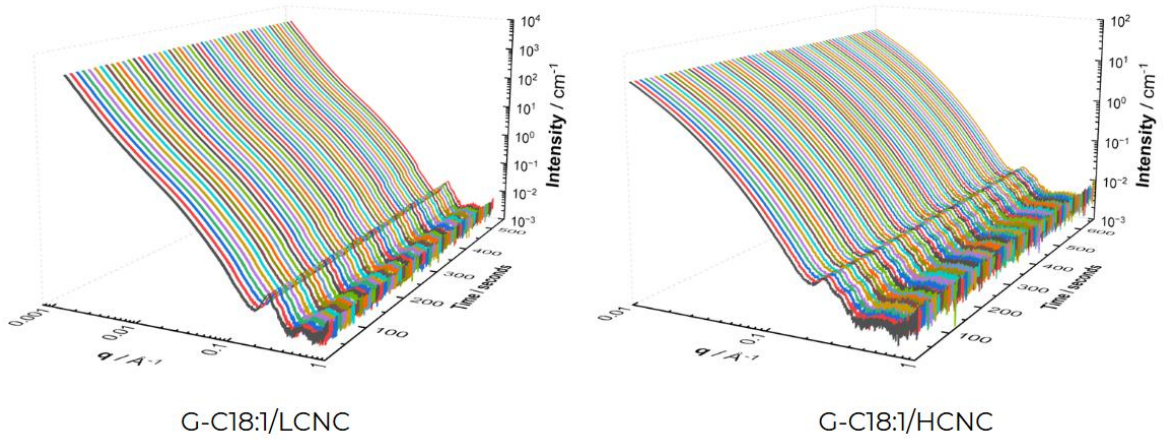

Figure S6. SAXS profiles tangential

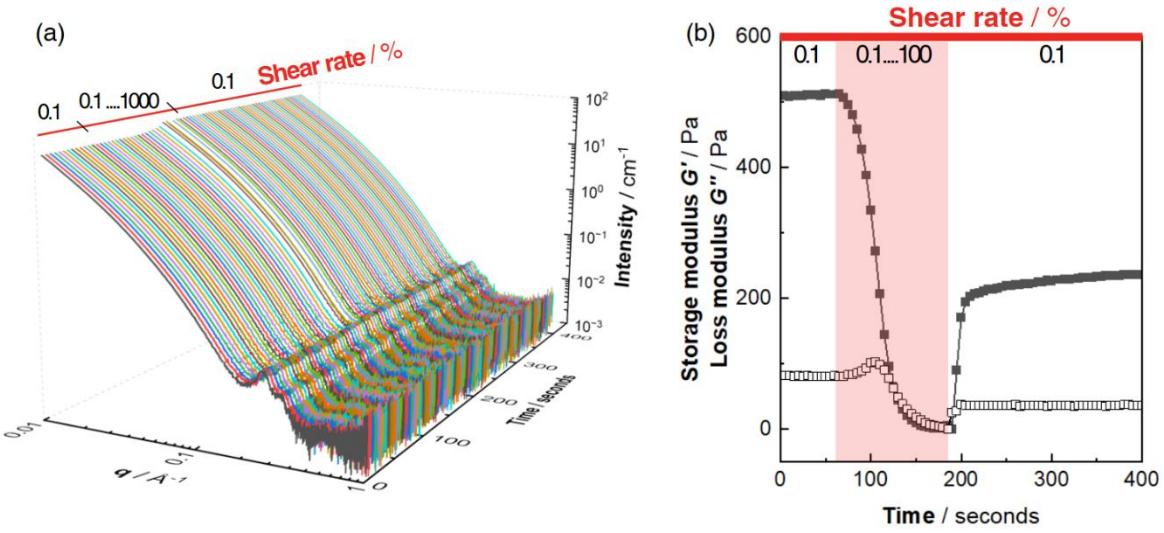

Figure S7. G-C18:1/HCNC 1m long shear rate variation

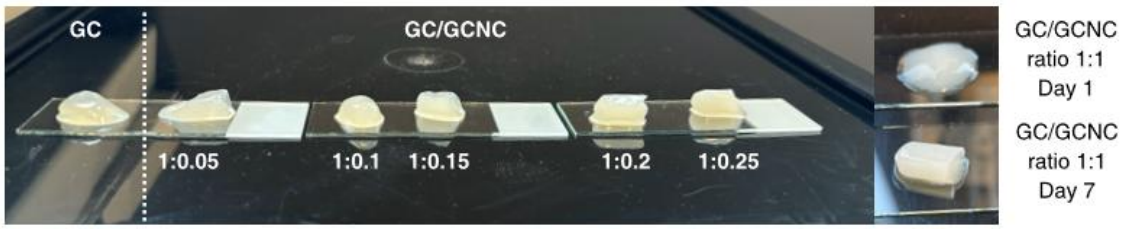

Figure S8. Could be used?

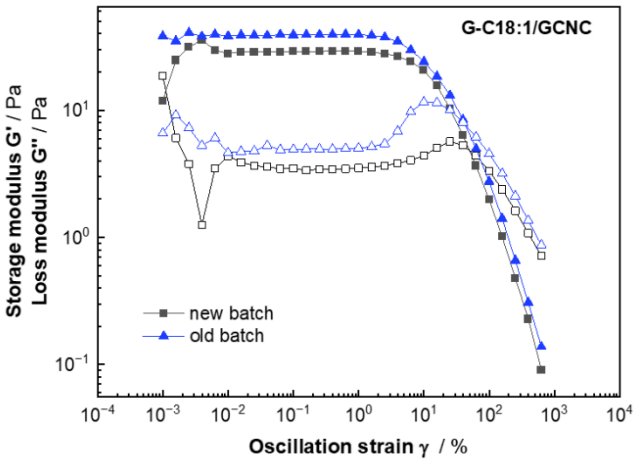

Figure S9. Could be used?